Brazilian Journal
of Chemical
Engineering

ISSN 0104-6632
Printed in Brazil
www.abeq.org.br/bjche

Vol. 36, No. 03, pp. 1319 - 1332, July - September, 2019
dx.doi.org/10.1590/0104-6632.20190363s20180036

SYNTHESIS, CHARACTERIZATION, ADSORPTION AND THERMODYNAMIC STUDIES OF PURE AND BINARY CO_2-N_2 MIXTURES ON OXYGEN ENRICHED NANOSTRUCTURED CARBON ADSORBENTS

Deepak Tiwari[1], Haripada Bhunia[1*] and Pramod K. Bajpai[1]

[1] Thapar Institute of Engineering & Technology, Department of Chemical Engineering, Patiala-147004, Punjab, India.
E-mail: deepak.tiwari@thapar.edu - ORCID: 0000-0001-7560-3189; E-mail: hbhunia@thapar.edu - ORCID: 0000-0002-9207-9179;
E-mail: pramod.iitk77@gmail.com - ORCID: 0000-0002-8371-5022

(Submitted: January 28, 2018 ; Revised: November 25, 2018 ; Accepted: December 19, 2018)

Abstract - Oxygen enriched porous carbons have been synthesized by a nanocasting technique using mesoporous zeolite as template and epoxy resin as precursor. Characterization results show the effect of the nanocasting technique on the development of heterogeneous surface, high basicity, and high surface area of 686.37 m^2g^{-1}, beneficial for CO_2 adsorption. Pure component adsorption isotherms were correlated with Langmuir, Sips, and dual-site Langmuir (DSL) models and found that Sips and DSL isotherm models fitted well, indicating thre heterogeneous nature of the adsorbent surface. Dynamic breakthrough data for the binary system CO_2-N_2 were obtained using a fixed-bed column at different adsorption temperatures (30-100 °C) and CO_2 feed concentrations (5-12.5% by volume). The developed adsorbent shows high adsorption capacity with complete regenerability over four adsorption/desorption cycles. Prediction of binary components (CO_2-N_2) was made by using extended Sips, extended DSL and IAST (ideal adsorbed solution theory) by utilizing pure component adsorption isotherm data. Experimental and predicted equilibrium data were compared with breakthrough curve data and it was found that the extended forms (Sips and DSL) indicated under-predicted CO_2 adsorption equilibria because of differences in adsorptive strengths of CO_2 and N_2 molecules. Also, adsorption equilibria were closely predicted using IAST theory. Asymmetric *x-y* diagrams from Raoult's law indicated positive deviation, implying that as the CO_2 gas phase molar fraction increases, total adsorbed amounts increase. Negative values of molar Gibbs free energy change suggested feasibility of the adsorption process. Formation of a more ordered configuration of CO_2 molecules on the adsorbent surface was seen as a higher heat of adsorption was exhibited for CO_2 as compared to N_2.
Keywords: Nanocasting, extended sips; Extended DSL; IAST; Selectivity.

INTRODUCTION

Nowadays, the world is facing tremendous challenges due to the increase in greenhouse gas emissions (mainly carbon dioxide), which causes a major global warming problem. The concentration of CO_2 has risen to 409 ppm level and continues to increase (2018). This increase in level is further affecting the global temperature, rise of sea levels as well as marine life. Measures required to be taken for the reduction of CO_2 concentration have turned out to be a necessity for our environment. Carbon capture and sequestration (CCS) is one of the effective and important technologies for controlling the increase in CO_2 concentration. Absorption, adsorption, membrane separation and cryogenic processes are

* Corresponding author: Haripada Bhunia - E-mail: hbhunia@thapar.edu

the various technologies that are being used for CCS. The conventional amine absorption technology for capture of CO_2 is efficient but presents a series of drawbacks like high energy requirements, equipment corrosion, and low efficiency. Many research groups, to improve adsorption capacity and CO_2 selectivity, modified the adsorbents by amine modification, but this has drawbacks. Modification caused blocking of adsorbent pores and adsorbents possess poor stability due to amine degradation. Alternatively, adsorption by solid adsorbents has gained attention due to its reduced energy penalty, high adsorption capacity, selectivity and fast kinetics coupled with good thermal and mechanical stability. Zeolites (Deng et al., 2012), activated carbons (Wang et al., 2012; Yoo et al., 2013), metal-organic frameworks (Bastin et al., 2008; Sumida et al., 2012), amine supported mesoporous materials (Melloa et al., 2011; Xu et al., 2009) are potential candidates used so far, but among these, carbon based adsorbents have been studied extensively due to their better properties like well-developed porous structures, high adsorption capacities, easy regenerability, fast kinetics coupled with high thermal and chemical stability. Moreover, the preparation of these carbon adsorbents can be carried out by using low-cost precursors and by using various preparation techniques like sol-gel, carbonization of carbon containing precursor and nanocasting techniques. Among the preparation techniques, nanocasting developed the materials having controlled pore structure used in this study. It is possible to improve the textural properties, it is less time-consuming and it is possible to control pore structure characteristics. In this technique, precursor is introduced into the template pores, carbonized and lastly the template is removed. Further, using heteroatoms like nitrogen, oxygen etc. (Tiwari et al., 2017a) in the carbon matrix increases their uptake capacity as well as improves the surface property and selectivity of the adsorbent towards CO_2. Therefore, carbon adsorbents obtained from high oxygen containing epoxy resin and using as template mesoporous MCM-41 can act as a potential adsorbent for selectively capturing CO_2.

Nitrogen-doped porous carbon monoliths synthesized by Hao et al. (2010) using pyrolysis of a copolymer of resorcinol, formaldehyde and lysine exhibited static CO_2 uptake of 3.13 mmol g^{-1} at 25 °C under a pure CO_2 atmosphere. N-enriched carbon adsorbents synthesized by Pevida et al. (2008) using melamine-formaldehyde resin showed CO_2 uptakes of 2.25 and 0.86 mmol g^{-1} at 25 °C and 75 °C, respectively, under a pure CO_2 environment. Literature shows that synthesis using direct carbonization of nitrogen/oxygen containing precursors shows poor textural properties of the adsorbent. Also, CO_2 adsorption capacities were determined under static conditions, which showed higher CO_2 uptake values but do not have much relevance to practical application in CO_2 capture. Therefore, this study, using a nanocasting technique and an adsorption study in a dynamic fixed bed adsorption system, is more relevant for flue gases.

Also, understanding of pure component adsorption isotherms is very crucial for assessing the capture capability of these adsorbents. Along with this, further knowledge of binary gas adsorption equilibria is important as it plays an important role in designing an economically feasible adsorption system for CO_2 capture. In the present study, using adsorption isotherm models and pure component adsorption equilibria data, adsorption equilibria of binary gas can be predicted (Do, 1998). This approach is preferred, otherwise it takes a lot of time for experimentation. To date, very few studies are available for predicting mixed-gas adsorption equilibria on carbon-based adsorbents from pure component adsorption. The few which have been studied are of pre-combustion CO_2 capture conditions like equilibrium CO_2 adsorption capacity and breakthrough time evaluated by García et al. (2011) on a commercial activated carbon adsorbent for the ternary system of $CO_2/N_2/H_2$ (pre-combustion CO_2 capture). In other work (Schell et al., 2012), pure component adsorption equilibria of CO_2, H_2, N_2 and binary equilibria of CO_2/H_2 and CO_2/N_2 were obtained gravimetrically on commercial activated carbon.

In this work. predicted binary gas adsorption data for CO_2 and N_2 on oxygen enriched nanostructured carbon pertaining to post-combustion capture conditions is compared with the experimental breakthrough data. For this, pure component (CO_2 and N_2) adsorption equilibria on prepared carbon were measured volumetrically at four different temperatures (30-100 °C). Langmuir, Sips and dual-site Langmuir (DSL) are the three different adsorption isotherm models used to fit the experimental data. Also, binary gas adsorption equilibria data, obtained from a fixed-bed adsorption system, were compared with the predicted data obtained from extended forms of pure component isotherm models. The present study is much more effective because it was performed in a dynamic fixed bed system in which we have evaluated CO_2 uptake from room temperature to high adsorption temperature along with regenerability.

MATERIALS AND METHODS

Materials

Oxygen enriched nanostructured carbon adsorbent (EZ-700) approximately ~ Rs 15,000 per kg, prepared from epoxy resin Lapox L-12 is DGEBA (Di Glycidyl Ether of Bisphenol-A) as polymeric precursor, was supplied by M/s Atul Ltd., Gujarat, India. The density and viscosity of resin are 1.1-1.2 g cm^{-3} and

9000-12000 mPa.s, respectively. Mesoporous zeolite (MCM-41) as template having a surface area of 800 m^2 g^{-1} and pore diameter of 3 nm (purchased from Tianjin Chemist Scientific Ltd., China) was used for the synthesis of adsorbents. Pure N_2 (99.995%) and CO_2 (99.999%) gases, procured from M/s Sigma Gases and Services (India), were used for pure and binary gas adsorption studies. Non-adsorptive gas, helium (He) of high purity (99.999%) from Sigma was used for outgassing the sample.

Characterization

Adsorbent preparation

The epoxy resin (80 g) and the template mesoporous zeolite (20 g) were mixed in 150 ml of pure ethanol followed by removal of excessive solvent by heating at 120 °C for 3 h to obtain templated resin. After this, carbonization and activation at 700 °C under N_2 and CO_2 atmospheres at a heating rate of 10 °C/min was performed. Flow of gases at 60 ml min^{-1} was maintained throughout the carbonization-activation. Then it was cooled to room temperature followed by dissolution of the sample in 40 wt.% NaOH solution for at least 24 h to remove the template. The obtained sample after washing is denoted as E-*T*, where *T* denotes the carbonization and activation temperature.

Adsorbent characterization

Elemental analysis (CHN) and oxygen content (determined by difference) was performed using a Thermo Scientific Flash 2000 organic elemental analyzer. Micrometrics ASAP 2020 sorption analyzer was used to obtain surface area and pore volume of the obtained sample. From N_2 isotherms, the specific surface area (S_{BET}) was calculated by using the Brunauer-Emmet-Teller (BET) equation. TEM images of samples were recorded on a JEOL JEM-2100 transmission electron microscope at operating voltage of 200 kV. The surface morphology of the samples was examined using a JEOL JSM-6510 LV scanning electron microscope. X-ray photoelectron spectroscopy (XPS) measurements were made to identify nitrogen moieties on samples in a Kratos axis ultra DLD system with an A1 K_α source. The anode potential and emission current were 15 kV and 10 mA, respectively.

Methods

Pure component adsorption measurement

Adsorption measurements of pure gases (CO_2 and N_2) on the nanostructured carbon adsorbent were performed using a Micrometrics ASAP 2010 volumetric analyzer at four different adsorption temperatures (30, 50, 75 and 100 °C) and pressures ranging from 0 to 1 atm using high purity CO_2 and N_2 gases. Before the analysis, carbon sample was degassed for 12 h under vacuum at 200 °C.

Binary component adsorption measurement

Binary equilibrium adsorption data were obtained using a fixed gas adsorption setup (Fig. 1) whose detailed description and procedure were reported in the previous paper (Tiwari et al., 2017b). The adsorption experiments were performed at approx. 1 atm in the fixed bed tests.

Adsorption/desorption experiments were performed by packing 2g of adsorbent in the fixed-bed column (internal diameter of 0.939 cm and height of 30 cm). Before this, adsorbent was kept overnight in the oven to remove moisture and other pre-adsorbed gases. Pretreatment of adsorbent under N_2 atmosphere (50 mL min^{-1}) was performed for 2 h at 200 °C in the column before carrying out adsorption. After this, adsorption was carried out by reducing the temperature to the desired adsorption temperature (30 to 100 °C) by passing different gas mixtures of CO_2 and N_2 at a total flow rate of 80 ml min^{-1} (evaluated at NTP), with varying CO_2 volumetric concentrations ranging from 5% to 12.5%. The exit CO_2 concentration was monitored by GC until the exit CO_2 concentration became equal to the inlet CO_2 concentration. At the end of the adsorption column, a gas chromatograph (GC 7890A, Agilent Technologies, US) is used to periodically monitor the CO_2 and N_2 concentrations. After performing the adsorption study, desorption was carried out by increasing the temperature to 200 °C under pure N_2 flow (50 ml min^{-1}).

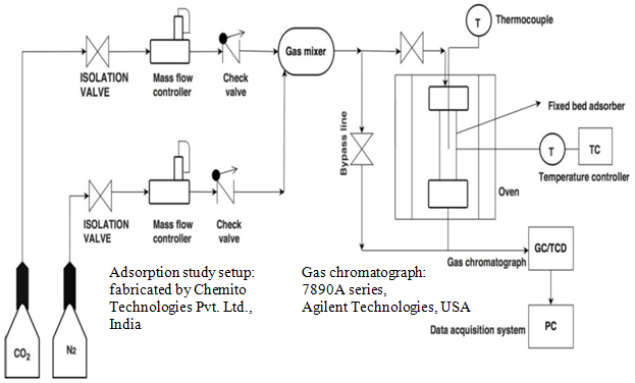

Figure 1. Schematic diagram of the CO_2 adsorption/desorption setup.

RESULTS AND DISCUSSION

Characterization of adsorbent

The prepared adsorbent shows an effect of template in development of nanostructured carbon in the range of 2-6 nm (TEM, Fig. 2a). SEM shows **a** nanocasting effect which is seen from **the** developed porosity having irregular and heterogeneous type pores (Fig. 2b) that can facilitate transport of CO_2 molecules towards the inner side of the adsorbent. N_2 adsorption/desorption show Type I and Type IV isotherms (Fig. 2c), showing

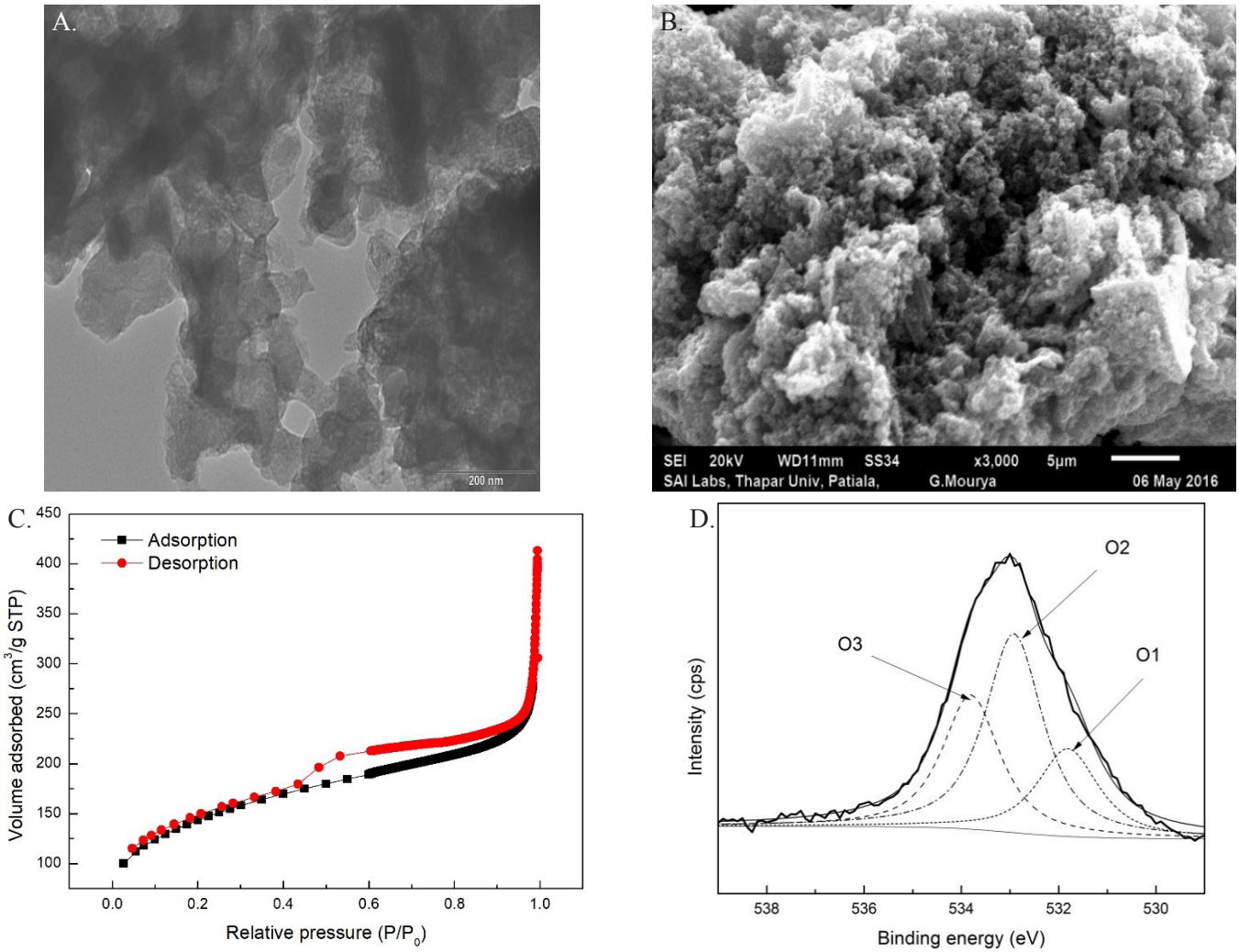

Figure 2. TEM image of (a) EZ-700, (b) SEM image of EZ-700, (c) N_2 adsorption-desorption isotherm of EZ-700, and (d) X-ray photoelectron spectra of EZ-700.

the presence of micro and mesopores with highest surface area of 686.37 m^2 g^{-1}. The oxygen content of the sample was 47.51% due to the presence of a higher amount (46.79 area %) of O2 (ether, alcohol) at binding energy of 532.92 eV (Fig. 2d) indicating higher basicity and selectivity towards CO_2.

Adsorption isotherm study

Pure component isotherms

Fig. 3 shows pure component adsorption-desorption (symbols) and the model predicted isotherms (as lines) on prepared oxygen enriched carbon adsorbent as a function of pressure at different adsorption temperatures (30-100 °C). It is seen that the adsorption of CO_2 and N_2 increases as pressure increases, while it decreases as temperature increases. CO_2 was found to adsorb more strongly on the adsorbent as compared to N_2 at all temperatures. Three pure component isotherm models (Langmuir, Sips and DSL) at different adsorption temperatures were used for fitting the experimental pure component adsorption data of CO_2 and N_2 on EZ-700. The corresponding model parameters along with SSE (sum of the squared relative errors) values are reported in Tables 1, 2 and 3.

The Langmuir adsorption isotherm model exhibits the correct asymptotic behavior as it approaches Henry's law in the low pressure range and is thermodynamically sound. However, this model is not able to explain well the adsorption behavior of CO_2 on EZ-700 at all adsorption temperatures as its SSE lie in the range of 19-22%. It deviated from experimental data at all pressures. On the other hand, both Sips and DSL isotherm models fit well as compared to Langmuir isotherm model as indicated by the SSE values (Sips <9.7% and DSL <3.24%). This signifies surface heterogeneity of the adsorbent. Similar results of conformity of these two models with CO_2 adsorption on carbon materials were shown by several research groups (Caldwell et al., 2015; García et al., 2013).

N_2 adsorption was well explained by all the three isotherm models and only a small difference is found between them. This is because of the linear shape

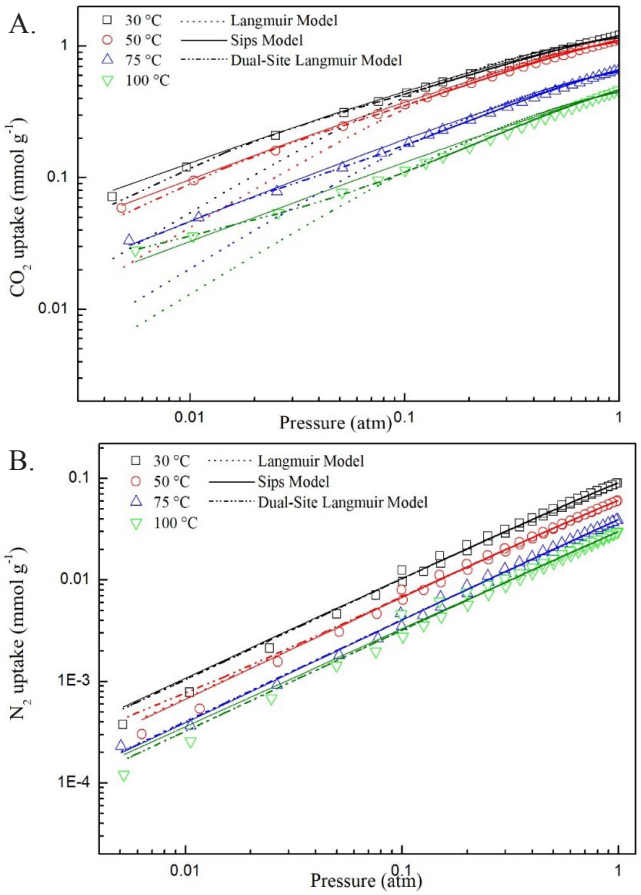

Figure 3. Experimental adsorption isotherms of (a) CO_2 and (b) N_2 on EZ-700 at different temperatures and their corresponding isotherm model fits.

Table 1. Langmuir isotherm model parameters for pure component adsorption on EZ-700 at different temperatures.

Component	Parameter	Temperature (°C)			
		30	50	75	100
CO_2	q_m (mmol g^{-1})	1.45	1.23	0.93	0.68
	b (atm^{-1})	3.89	3.03	2.25	1.97
	SSE (%)	22.31	19.83	19.65	19.20
	b_o (atm^{-1})	0.09			
	B (kJ mol^{-1})	-9.36			
N_2	q_m (mmol g^{-1})	1.37	0.70	0.55	0.43
	b (atm^{-1})	0.15	0.12	0.08	0.03
	SSE (%)	4.02	5.66	6.84	7.55
	b_o (atm^{-1})	0.0005			
	B (kJ mol^{-1})	-14.35			

of the N_2 isotherm that can be fitted well with all aforementioned isotherm models (Caldwell et al., 2015).

CO_2 affinity towards the adsorbent surface is higher as compared to N_2 as observed from higher values of b in Tables 1, 2 and 3. Moreover, higher q_m values of CO_2 adsorption than N_2 were obtained with all three isotherm models. N_2 considers both the adsorption sites as equal free-energy sites which are confirmed by similar values of the parameters b_1 and b_2 in the DSL isotherm. Therefore, there will be no energetic site-matching issue and CO_2 (component 1) will see site 1 as high free energy site and site 2 as low free energy site. So, there will be only one value of adsorbed amount for an adsorbate at a given temperature and gas composition conditions. It is seen that the parameter b (Langmuir and Sips model) and b_1 and b_2 (Dual-site Langmuir) values decreased with increasing temperature, signifying the exothermic nature of the adsorption process. The Sips isotherm model parameter value c shows a deviation in value from unity, indicating heterogeneity of the adsorption process.

Table 2. Sips isotherm model parameters for pure component adsorption on EZ-700 at different temperatures.

Component	Parameter	Temperature (°C)			
		30	50	75	100
CO_2	q_m (mmol g^{-1})	2.80	2.60	2.06	2.40
	b (atm^{-c})	0.80	0.66	0.47	0.24
	c	1.66	1.62	1.58	1.53
	SSE (%)	2.84	3.35	5.59	9.70
	b_o (atm^{-c})	0.002			
	B (kJ mol^{-1})	-15.70			
N_2	q_m (mmol g^{-1})	0.87	0.81	0.50	0.27
	b (atm^{-c})	0.14	0.13	0.05	0.01
	c	1.01	0.99	0.99	1.04
	SSE (%)	6.84	5.83	3.42	1.24
	b_o (atm^{-c})	0.0072			
	B (kJ mol^{-1})	-31.14			

Table 3. Dual-site Langmuir isotherm model parameters for pure component adsorption on EZ-700 at different temperatures.

Component	Parameter	Temperature (°C)			
		30	50	75	100
CO_2	$q_{1,m}$ (mmol g^{-1})	1.60	1.14	0.20	0.04
	$q_{2,m}$ (mmol g^{-1})	0.29	1.65	0.92	0.07
	b_1 (atm^{-1})	55.34	32.49	21.08	11.08
	b_2 (atm^{-1})	1.82	1.26	0.93	0.88
	SSE (%)	2.72	2.70	2.64	3.24
	$b_{o,1}$ (atm^{-1})	0.273			
	$b_{o,2}$ (atm^{-1})	0.00017			
	B (kJ mol^{-1})	48.06			
	E_2 (kJ mol^{-1})	-30.15			
N_2	$q_{1,m}$ (mmol g^{-1})	0.68	0.35	0.28	0.21
	$q_{2,m}$ (mmol g^{-1})	0.68	0.35	0.28	0.21
	b_1 (atm^{-1})	0.15	0.12	0.06	0.03
	b_2 (atm^{-1})	0.15	0.12	0.06	0.03
	SSE (%)	2.02	4.66	3.84	4.55
	$b_{o,1}$ (atm^{-1})	0.032			
	$b_{o,2}$ (atm^{-1})	0.00046			
	B (kJ mol^{-1})	43.676			
	E_2 (kJ mol^{-1})	-14.354			

Binary component isotherms

Sips and DSL isotherm models were used for binary component adsorption as these models properly explain the pure component adsorption behavior. Also, IAST

(ideal adsorbed solution theory) was only applied for the above two isotherms. Breakthrough curves of the binary mixture (CO_2 and N_2) at different temperatures (30 °C and 50 °C) and at 12.5% CO_2 concentration (by volume) are shown in Fig. 4. A hump in the C/C_O value, i.e., >1, is seen from Fig. 4, which indicates that nitrogen comes out first and gets less adsorbed as compared to CO_2. A maximum adsorption capacity of 0.65 mmol g^{-1} under 12.5% CO_2 concentration at 30 °C is obtained for this sample. Also, the developed adsorbent exhibits quick and complete regenerability over four adsorption/desorption cycles. The obtained capacity is somewhat similar to CO_2 uptake obtained for activated carbon (0.61 mmol g^{-1}) which was prepared using coal tar pitch and furfural by steam activation (Balsamo et al., 2013). But, the demerits of their study is that CO_2 uptake was evaluated using a volumetric apparatus under static conditions which does not give the real picture for CO_2 capture in a dynamic system.

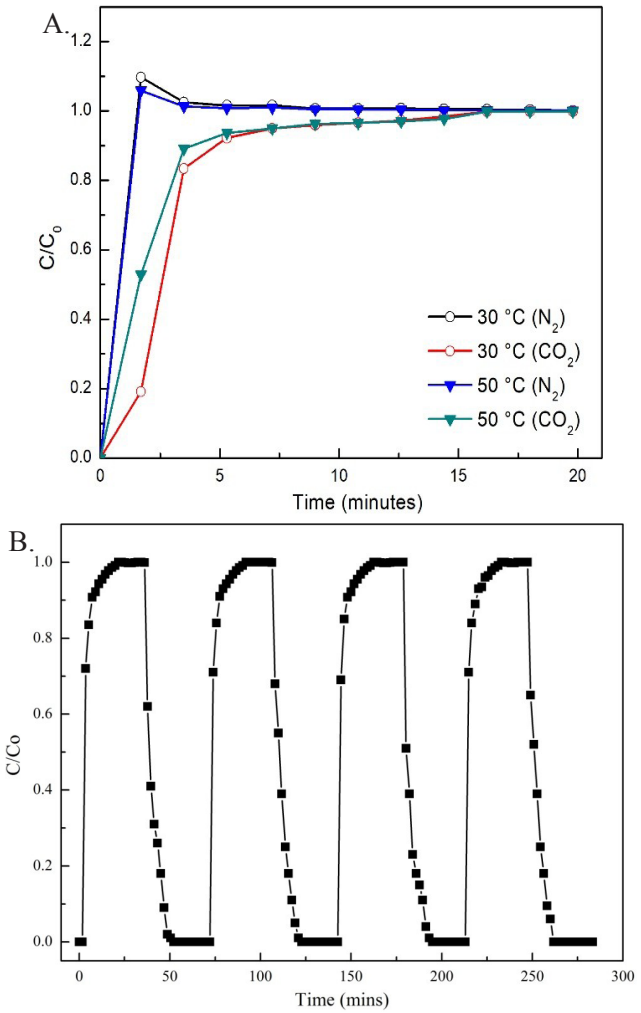

Figure 4. Breakthrough curves of CO_2 (closed symbols) and N_2 (opensymbols) for 12.5% CO_2 in N_2, on EZ-700 at 30 °C and 50 °C (b) Multi-cycle CO_2 adsorption-desorption concentration profile of EZ-700 at 30 ºC.

Partial and total adsorbed amounts of CO_2 and N_2 on EZ-700 at different adsorption temperatures are shown in Fig. 5. Sips, DSL, IAST-Sips and IAST-DSL isotherm predictions and experimental values of CO_2 adsorbed are presented in Table 4.

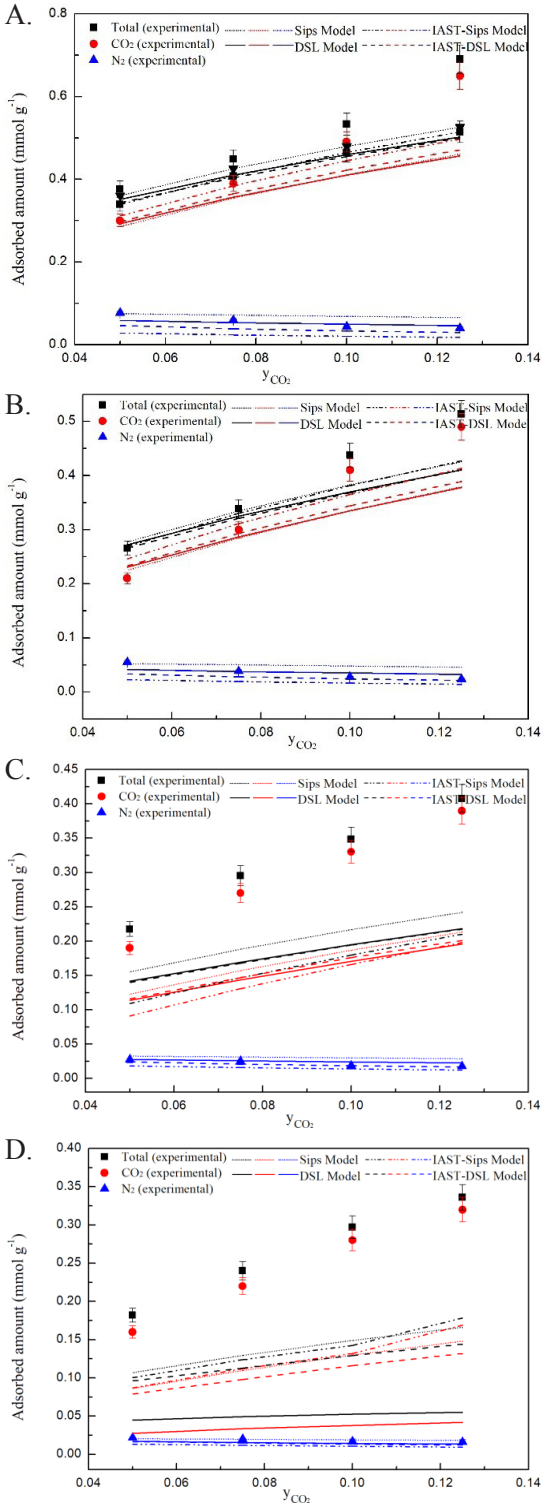

Figure 5. Binary adsorption isotherms for CO_2-N_2 mixtures on EZ-700 at (a) 30 °C, (b) 50 °C, (c) 75 °C, and (d) 100 °C (symbols represent experimental data and lines represent model predicted data).

Table 4. Comparison of experimental and predicted binary system CO_2 adsorption capacities on EZ-700 based on binary component adsorption isotherms.

Temperature	CO_2 mole fraction in feed	CO_2 adsorption capacity (mmol g^1)				
		Experimental	Sips model	DSL model	IAST-Sips model	IAST-DSL model
30 °C	0.050	0.30	0.29	0.29	0.31	0.30
	0.075	0.39	0.35	0.36	0.38	0.37
	0.100	0.49	0.41	0.41	0.45	0.42
	0.125	0.65	0.64	0.64	0.63	0.67
50 °C	0.050	0.21	0.23	0.23	0.25	0.23
	0.075	0.30	0.28	0.29	0.31	0.29
	0.100	0.41	0.34	0.34	0.39	0.37
	0.125	0.49	0.38	0.38	0.50	0.46
75 °C	0.050	0.19	0.12	0.11	0.19	0.16
	0.075	0.27	0.16	0.14	0.26	0.24
	0.100	0.33	0.19	0.17	0.36	0.34
	0.125	0.39	0.21	0.19	0.40	0.35
100 °C	0.050	0.16	0.09	0.07	0.15	0.13
	0.075	0.22	0.11	0.08	0.25	0.21
	0.100	0.28	0.13	0.09	0.26	0.22
	0.125	0.32	0.15	0.13	0.27	0.29

It can be seen that both Sips and DSL show different predicted values of CO_2 adsorbed amount. The predicted value of CO_2 obtained from the Sips equation as compared to the DSL equation is higher at 75 and 100 °C**.** On the other hand, IAST-Sips shows higher value of the CO_2 adsorbed amount as compared to IAST-DSL at all temperatures. However, the IAST forms of these two isotherm models show somewhat similar values for the CO_2 capacity obtained experimentally. Similar kinds of observations were seen for predicted N_2 uptake values by these isotherm models. Therefore, it can be concluded that, IAST forms of these isotherm models show similar predicted CO_2 capacities as those of experimental data obtained from binary breakthrough curves. Total and partial adsorbed amounts were highly under predicted by all these models with maximum under-estimation by Sips and IAST based Sips isotherm models for CO_2 and N_2 adsorption, respectively.

Experimental and model predicted molar fractions of CO_2 in the adsorbed phase vs. mole fraction of CO_2 in gas phase at different adsorption temperatures for the CO_2-N_2 binary system were determined and shown in Fig. 6. Maximum deviation for the DSL model at

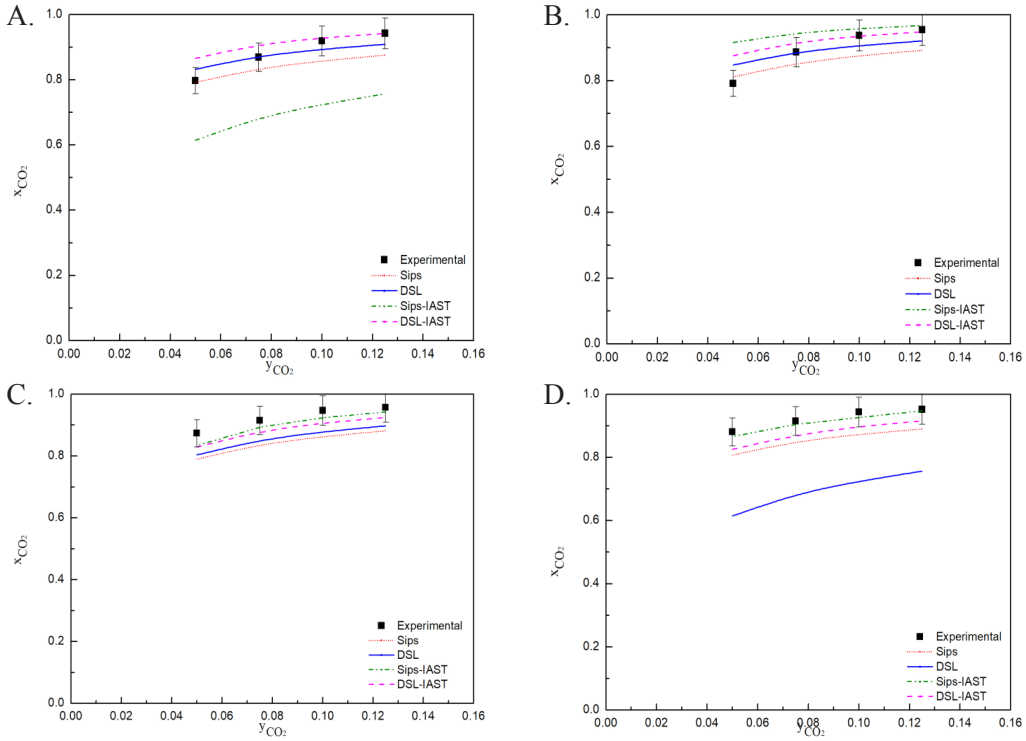

Figure 6. *x-y* diagrams for binary adsorption of CO_2 and N_2 on EZ-700 at (a) 30 °C, (b) 50 °C, (c) 75 °C, and (d) 100 °C.

100 °C and for Sips at 100 °C in predicting *x* for a given *y* is observed. However, for IAST based models, except at 30 °C (under predicted), they followed closely the experimental data for CO_2 mole fraction. Also, symmetric *x-y* diagrams along with rising total adsorbed amount with mole fraction in the gas phase are exhibited by gas mixtures showing ideal behavior at equilibrium (Bakhtyari and Mofarahi, 2014). Adsorption of the CO_2-N_2 gas mixture on EZ-700 does not show a symmetric *x-y* diagram, though total adsorbed amount increased with gas phase mole fraction. This suggests that carbon dioxide and nitrogen do not form ideal adsorptive mixtures on mesoporous carbon EZ-700.

Comparison of adsorption selectivity calculated experimentally from breakthrough curves under dynamic conditions and obtained from various isotherm models is also made. Experimental and predicted values of adsorption selectivity are shown in Table 5. Sips and DSL isotherm models show lower values, while IAST-Sips and IAST-DSL, except at 50 °C, show lower values of selectivity for CO_2 over N_2. This shows the inability of binary component adsorption isotherms to predict mixed gas adsorption equilibria. It is also observed that, with the increase of CO_2 concentration, selectivity obtained from breakthrough curves increases, while for Sips and DSL it decreases. IAST-Sips and IAST-DSL show a smaller decrease in selectivity over the complete range of CO_2 concentration.

It is noted that the prediction of adsorption equilibria from IAST isotherm models for the binary component system was not correct because they vary in their size, polarity and most importantly they do not have the same equilibrium adsorption capacity. Also, in the case of heterogeneous adsorbents, IAST led to inadequate prediction of adsorption capacities. It provides relatively accurate multi-component behavior of systems such as CH_4-CO_2, CH_4-N_2, noble gases etc. (Walton and Sholl, 2015). CO_2 adsorbs more strongly as compared to N_2. Therefore, in the present study the difference in their adsorption levels is the main reason for under predicted adsorption behavior of the CO_2-N_2 system.

IAST has been extensively used by researchers for predicting mixed-gas adsorption equilibria, mostly in high pressure regions for pre-combustion capture application. Jeon *et al*. (2004), using NaX zeolite, studied CO_2 separation from a CO_2/N_2 mixture in a PSA system. The IAST model was able to predict proper behavior, but the extended Langmuir isotherm was unable to predict CO_2-N_2 adsorption behavior properly. Another study by Caldwell et al. (2015) was related to CO_2-N_2 equilibrium adsorption capacities obtained from breakthrough curves using fixed-bed experiments under high pressure conditions for CO_2 capture application. Sips and IAST-DSL models showed under predicted CO_2 uptake and the dual-site Langmuir isotherm model showed proper behavior for CO_2-N_2 system on activated carbons.

Thermodynamic study

Using the Sips isotherm model and equations S(18-21), thermodynamic parameters for CO_2 and N_2 adsorption on EZ-700 were calculated numerically. Thermodynamic parameters for adsorption at 30 °C only are shown in Fig.7. The negative value of the integral molar Gibbs free energy change at all temperatures indicates feasibility and spontaneity of the process. A higher amount of isothermal work is required for packing more adsorbate molecules into the adsorbent's cavity as compared to the initial adsorption, which was confirmed from the increase of pressure and fall in values of both CO_2 and N_2. At 0.08 mmol g^{-1} coverage, ΔG on EZ-700 for CO_2 and N_2 were -2.13 and -2.57 kJ mol^{-1}, respectively, indicating less amount of work required for loading of CO_2 on EZ-700 than for N_2 (Yi et al., 2013).

Table 5. Experimental and isotherm model predicted selectivities for CO_2-N_2 binary system on EZ-700.

Temperature	CO_2 mole fraction in feed	Selectivity				
		Experimental	Sips model	DSL model	IAST-Sips model	IAST-DSL model
30 °C	0.050	74.63	72.39	94.37	30.28	122.98
	0.075	81.91	60.98	82.49	26.18	117.60
	0.100	102.28	54.08	75.14	23.57	115.33
	0.125	114.13	49.35	70.12	21.78	114.10
50 °C	0.050	71.99	81.55	105.48	206.39	133.71
	0.075	96.17	69.93	93.46	201.47	129.72
	0.100	133.75	62.83	86.13	201.48	128.45
	0.125	146.26	57.93	81.13	204.65	128.22
75 °C	0.050	131.21	71.50	77.74	95.06	92.21
	0.075	131.93	61.95	69.04	102.76	87.15
	0.100	160.30	56.05	64.26	108.63	85.98
	0.125	155.22	51.95	61.20	114.39	85.21
100 °C	0.050	140.37	79.80	30.28	123.39	90.06
	0.075	133.68	68.47	26.18	117.16	81.30
	0.100	150.60	61.53	23.57	113.43	77.90
	0.125	138.94	56.73	21.78	126.51	75.89

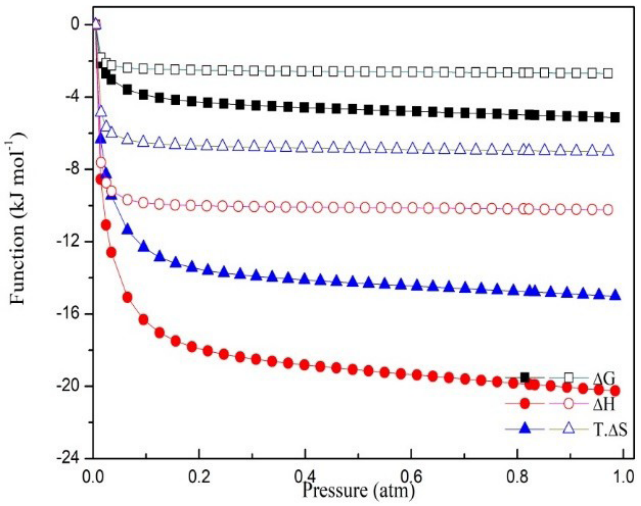

Figure 7. Thermodynamic functions (ΔG, ΔH and $\Delta S \times T$) for CO_2 (closed symbols) and N_2 (open symbols) on EZ-700 at 30 °C.

Negative values of $\Delta S \times T$ over the complete pressure range at 30 °C indicate random to more orderly adsorption for CO_2 and N_2 on the adsorbent surface.

$\Delta S \times T$ for N_2 decreases with pressure and was almost constant for CO_2. A decrease in the cavity's free space with increase in adsorbate molecule loading was also observed, signifying that N_2 adsorption on EZ-700 is homogenous. CO_2 adsorption on EZ-700 is heterogeneous which is seen from the small increase in the amount of entropy in the low pressure range (Deng et al., 2012; Zhou et al., 2012). At 0.08 mmol g^{-1}, $\Delta S \times T$ values for CO_2 and N_2 adsorption on EZ-700 at 30 °C are -14.22 and -8.53 kJ mol^{-1}, respectively, indicating a lower degree of disorder for CO_2 and higher for N_2. Lower degree of freedom of constrained CO_2 after it gets adsorbed onto carbon adsorbent is also confirmed from this. Efficient packing of CO_2 in the adsorbent cavity is because of localized adsorption, which is due to its higher quadruple moment than N_2. These quadruple moments of both CO_2 and N_2 interact with electrostatic-field gradients, thereby causing increased rotation and hence orientation of these molecules producing more efficient packing and this is more evident for CO_2 than N_2 due to its about three-fold larger quadruple moment than N_2 (Ridha and Webley, 2010).

Negative values of the integral molar enthalpy change confirmed the exothermic nature of the adsorption of CO_2 and N_2 on EZ-700 at 30 °C. A similar pattern was seen for molar enthalpy change and entropy change. With the increase of pressure from 0.01 to 1 atm, molar enthalpy changes of CO_2 on EZ-700 ranged from -11.58 to -23.20 kJ mol^{-1}, while for N_2 they varied from -6.61 to -11.21 kJ mol^{-1}. This indicates a more effective molecular packing, and higher amount of release of heat. Similar observations were seen for activated carbons like Maxsorb III (-20.37 kJ mol^{-1}) (Saha et al., 2011), coal based activated carbon (21.89 kJ mol^{-1}) (Yi et al., 2014), and activated carbon beads (-23.17 kJ mol^{-1}) (Shen et al., 2010).

As these parameters are calculated using the isotherm equation for each component, it is not possible to calculate them for binary system adsorption because there is no isotherm available to accurately predict the binary system equilibria.

Isosteric heat of adsorption for the adsorption of pure CO_2 from equilibrium isotherms is calculated by using the Clausius-Clapeyron equation S(21) and is shown in Fig. 8. The average value of isosteric heat of adsorption (Q_{st}) for CO_2 on EZ-700 was calculated to be ca. 34.82 kJ mol^{-1} which is in agreement with the available value in thre literature for carbon adsorbents (Caldwell et al., 2015; Shen et al., 2010; Yi et al., 2014). An almost constant Q_{st} value was seen at different surface loadings. This is in line with the assumption of the DSL adsorption model wherein Q_{st} is independent of adsorbate loading on the adsorbent surface. Also, this supports the accurate prediction of CO_2 adsorption on EZ-700 by the DSL isotherm model.

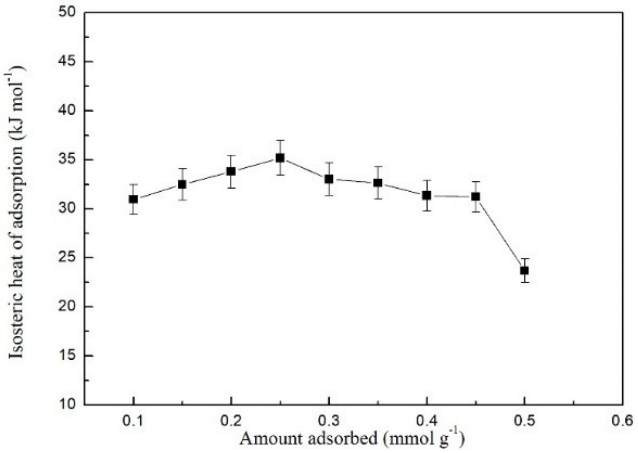

Figure 8. Isosteric heat of adsorption of pure CO_2 from equilibrium isotherms on EZ-700.

CONCLUSIONS

Oxygen enriched nanostructured low-cost carbon having heterogeneous pores and high basicity is successfully developed using a nanocasting technique. Sips and DSL isotherm models provide the best fit over the entire pressure range. Adsorption equilibria of binary component CO_2 and N_2 at four different adsorption temperatures (30-100 °C) and CO_2 concentrations (5-12.5%) have been measured on EZ-700 using a fixed bed column. The adsorbent shows 0.636 mmol g^{-1} adsorption capacity with complete regenerability over four adsorption/desorption cycles. For predicting binary component adsorption equilibria, extended Sips, extended dual-site Langmuir, IAST-based Sips and IAST-based DSL models have been

used. Unlike Sips and DSL, IAST-based Sips and IAST-based DSL closely predicted the adsorption behavior of the binary component. Neither selectivity nor total adsorbed amount can be explained properly by these models because of high adsorption strength and the heterogeneous adsorbent surface of one component as compared to the other. Overall, it can be concluded that binary component adsorption equibria are important for real systems. These help in better selecting the appropriate model for simulation of gas phase adsorption systems.

Molar Gibbs free energy change, entropy change, and enthalpy change for pure components signify a spontaneous, exothermic and feasible nature of adsorption process. Effective packing of CO_2 molecules in the cavities of carbon adsorbents has been confirmed by the higher amount of heat generation for CO_2. Higher chemical potential and higher pressure are required by N_2 as compared to CO_2 to load carbon on its surface.

ACKNOWLEDGEMENTS

The author would like to greatly acknowledge financial support provided by the Department of Science and Technology (DST) (scheme no. DST/IS-STAC/CO_2-SR-154/12(G).

REFERENCES

CO_2.earth (2017). https://www.co2.earth/.

Bakhtyari, A., Mofarahi, M. Pure and binary adsorption equilibria of methane and nitrogen on Zeolite 5A. J. Chem. Eng. Data, 59, 626-639 (2014). https://doi.org/10.1021/je4005036

Balsamo, M., Budinova, T., Erto, A., Lancia, A., Petrova, B., Petrov, N., Tsyntsarski, B. CO_2 adsorption onto synthetic activated carbon: kinetic, thermodynamic and regeneration studies. Sep. Purif. Technol. 116, 214-221 (2013). https://doi.org/10.1016/j.seppur.2013.05.041

Bastin, L., Barcia, P.S., Hurtado, E.J., Silva, J.A.C., Rodrigues, A.E., Chen, B. A microporous metal-organic framework for separation of CO_2/N_2 and CO_2/CH_4 by fixed-bed adsorption. J. Phy. Chem. C, 112, 1575-1581 (2008). https://doi.org/10.1021/jp077618g

Caldwell, S.J., Al-Duri, B., Sun, N., Sun, C.-G., Liu, H., Snape, C.E., Li, K., Wood, J. Carbon dioxide separation from nitrogen/hydrogen mixtures over activated carbon beads: Adsorption isotherms and breakthrough studies. Energy Fuels, 29, 3796-3807 (2015). https://doi.org/10.1021/acs.energyfuels.5b00164

Deng, H., Yi, H., Tang, X., Yu, Q., Ning, P., Yang, L. Adsorption equilibrium for sulfur dioxide, nitric oxide, carbon dioxide, nitrogen on 13X and 5A zeolites. Chemical Engineering Journal, 188, 77-85 (2012). https://doi.org/10.1016/j.cej.2012.02.026

Do, D.D. Adsorption Analysis: Equilibria and Kinetics. Imperial College Press (1998). https://doi.org/10.1142/9781860943829

García, S., Gil, M., Martín, C., Pis, J., Rubiera, F., Pevida, C. Breakthrough adsorption study of a commercial activated carbon for pre-combustion CO_2 capture. Chemical Engineering Journal, 171, 549-556 (2011). https://doi.org/10.1016/j.cej.2011.04.027

García, S., Pis, J.J., Rubiera, F., Pevida, C. Predicting mixed-gas adsorption equilibria on activated carbon for precombustion CO_2 Capture. Langmuir, 29, 6042-6052 (2013). https://doi.org/10.1021/la4004998

Hao, G.P., Li, W.C., Qian, D., Lu, A.H. Rapid Synthesis of Nitrogen-doped porous carbon monolith for CO_2 capture. Adv. Mater., 22, 853-857 (2010). https://doi.org/10.1002/adma.200903765

Jeon, J.-K., Ihm, S.-K., Park, Y.-K., Kim, J.S., Kim, S.D., Kim, S., Kim, J.M., Kim, S.-S., Yoo, K.-S. Effect of Isotherm selection on performance prediction of CO_2 PSA process, in: Sang-Eon Park, J.-S.C., Kyu-Wan, L. (Eds.), Studies in Surface Science and Catalysis. Elsevier, pp. 547-550 (2004). https://doi.org/10.1016/S0167-2991(04)80312-4

Melloa, M.R., Phanon, D., Silveira, G.Q., Llewellyn, P.L., Ronconi, C.M. Amine-modified MCM-41 mesoporous silica for carbon dioxide capture. Microporous Mesoporous Mater., 143, 174-179 (2011). https://doi.org/10.1016/j.micromeso.2011.02.022

Myers, A. L, Prausnitz, J.M. Thermodynamics of mixed gas adsorption. AICHE J., 11, 121-127 (1965). https://doi.org/10.1002/aic.690110125

Pevida, C., Drage, T.C., Snape, C.E. Silica-templated melamine-formaldehyde resin derived adsorbents for CO_2 capture. Carbon, 46, 1464-1474 (2008). https://doi.org/10.1016/j.carbon.2008.06.026

Ridha, F.N., Webley, P.A. Entropic effects and isosteric heats of nitrogen and carbon dioxide adsorption on chabazite zeolites. Microporous Mesoporous Mater., 132, 22-30 (2010). https://doi.org/10.1016/j.micromeso.2009.07.025

Saha, B.B., Jribi, S., Koyama, S., El-Sharkawy, I.I. Carbon dioxide adsorption isotherms on activated carbons. J. Chem. Eng. Data, 56, 1974-1981 (2011). https://doi.org/10.1021/je100973t

Schell, J., Casas, N., Pini, R., Mazzotti, M. Pure and binary adsorption of CO_2, H_2, and N_2 on activated carbon. Adsorption, 18, 49-65 (2012). https://doi.org/10.1007/s10450-011-9382-y

Shen, C., Grande, C.A., Li, P., Yu, J., Rodrigues, A.E. Adsorption equilibria and kinetics of CO_2 and N_2 on activated carbon beads. Chemical Engineering Journal, 160, 398-407 (2010). https://doi.org/10.1016/j.cej.2009.12.005

Sumida, K., Rogow, D.L., Mason, J.A., McDonald, T.M., Bloch, E.D., Herm, Z.R., Bae, T.H., Long, J.R. Carbon dioxide capture in metal-organic frameworks. Chem. Rev., 112, 724-781 (2012). https://doi.org/10.1021/cr2003272

Tiwari, D., Bhunia, H., Bajpai, P.K. Synthesis of nitrogen enriched porous carbons from urea formaldehyde resin and their carbon dioxide adsorption capacity. J. CO_2 Utilization, 21, 302-313 (2017a). https://doi.org/10.1016/j.jcou.2017.08.002

Tiwari, D., Goel, C., Bhunia, H., Bajpai, P.K. Dynamic CO_2 capture by carbon adsorbents: kinetics, isotherm and thermodynamic studies. Sep. Purif. Technol., 181, 107-122 (2017b). https://doi.org/10.1016/j.seppur.2017.03.014

Walton, K.S., Sholl, D.S. Predicting multicomponent adsorption: 50 years of the ideal adsorbed solution theory. AIChE J., 61, 2757-2762 (2015). https://doi.org/10.1002/aic.14878

Wang, D., Ma, X., Sentorun-Shalaby, C., Song, C. Development of carbon-based "Molecular Basket" Sorbent for CO_2 capture. Ind. Eng. Chem. Res., 51, 3048-3057 (2012). https://doi.org/10.1021/ie2022543

Xu, X., Zhao, X., Sun, L., Liu, X. Adsorption separation of carbon dioxide, methane and nitrogen on monoethanol amine modified β-zeolite. J. Nat. Gas Chem., 18, 167-172 (2009). https://doi.org/10.1016/S1003-9953(08)60098-5

Yi, H., Li, F., Ning, P., Tang, X., Peng, J., Li, Y., Deng, H. Adsorption separation of CO_2, CH_4, and N_2 on microwave activated carbon. Chemical Engineering Journal, 215-216, 635-642 (2013). https://doi.org/10.1016/j.cej.2012.11.050

Yi, H., Wang, Z., Liu, H., Tang, X., Ma, D., Zhao, S., Zhang, B., Gao, F., Zuo, Y. Adsorption of SO_2, NO, and CO_2 on activated carbons: Equilibrium and thermodynamics. J. Chem. Eng. Data, 59, 1556-1563 (2014). https://doi.org/10.1021/je4011135

Yoo, H.-M., Lee, S.-Y., Park, S.-J. Ordered nanoporous carbon for increasing CO_2 capture. J. Solid State Chem., 197, 361-365 (2013). https://doi.org/10.1016/j.jssc.2012.08.035

Zhou, X., Yi, H., Tang, X., Deng, H., Liu, H. Thermodynamics for the adsorption of SO_2, NO and CO_2 from flue gas on activated carbon fiber. Chemical Engineering Journal, 200-202, 399-404 (2012). https://doi.org/10.1016/j.cej.2012.06.013

APPENDIX - THEORY

Pure component isotherm

Langmuir, Sips and Dual-site isotherm models were used to predict adsorption equilibrium of pure gases (CO_2 and N_2) on prepared oxygen enriched carbon.

Langmuir isotherm

$$q_e = \frac{q_m b P}{1 + bP} \tag{A.1}$$

where q_e (mmol g^{-1}) is the equilibrium adsorption capacity, q_m (mmol g^{-1}) is the maximum monolayer capacity, b (atm^{-1}) is the affinity of adsorbed molecules towards the adsorbent surface and P is the total pressure.

Sips isotherm model

$$q_e = \frac{q_m b P^{1/c}}{1 + bP^{1/c}} \tag{A.2}$$

Dual-site Langmuir model

$$q_e = \frac{q_{1,m} b_1 P}{1 + b_1 P} + \frac{q_{2,m} b_2 P}{1 + b_2 P} \tag{A.3}$$

where $q_{1,m}$ and $q_{2,m}$ are the saturation capacities of the adsorbate at sites 1 and 2, respectively, b_1 and b_2 are the affinity parameters on sites 1 and 2, respectively.

Temperature dependent parameter for Langmuir isotherm

$$b = b_o e^{-(B/RT)} \tag{A.4}$$

where b_o is the adsorption affinity at the reference temperature, and B (J mol^{-1}) is the heat of adsorption.

Temperature dependent parameter for Dual-site isotherm

$$b_j = b_{o,j} e^{E_j/RT} \tag{A.5}$$

where j is the energy level of site 1 or 2, $b_{o,j}$ is the adsorption affinity at the reference temperature and E_j is the corresponding adsorption energy.

Error calculation

$$\mathrm{SSE}(\%) = \sqrt{\frac{\Sigma\left[\left(q_{e,exp} - q_{e,pred}\right)/q_{e,exp}\right]^2}{N-1}} \times 100 \tag{A.6}$$

where $q_{e,exp}$ and $q_{e,pred}$ are the experimental and model predicted amounts of adsorbate adsorbed, respectively, and N = total number of data points.

Binary component isotherm

In the present study, two approaches were used for the prediction of adsorption equilibria of the

binary system (CO_2 and N_2) using pure component adsorption isotherm parameters. In the first approach, the models which properly fitted the pure component data were extended to binary component adsorption isotherms and, in the other. ideal adsorbed solution theory (IAST) model was used to derive binary system isotherms from pure component adsorption isotherms. Further, these predicted isotherms are compared with the measured binary system isotherms.

Extended Sips isotherm model

$$q_{e,i} = \frac{q_{m,i} b_i P_i^{1/c_i}}{1 + \sum_{j=1}^{N_C} b_j P_j^{1/c_i}} \tag{A.7}$$

where i is the component for which isotherm is evaluated, and $q_{e,i}$ is the equilibrium adsorption capacity of component i in the mixture.

Extended dual-site Langmuir isotherm model

$$q_{e,i} = \frac{q_{1,m,i} b_{1,i} P_i}{1 + \sum_{j=1}^{N_C} b_{1,j} P_j} + \frac{q_{2,m,i} b_{2,i} P_i}{1 + \sum_{j=1}^{N_C} b_{2,j} P_j} \tag{A.8}$$

Ideal adsorbed solution theory (IAST)

Another model, which is given by Myers and Prausnitz (1965), for prediction of adsorption equilibria of a binary system using pure component adsorption isotherms is Ideal adsorbed solution theory (IAST). This model depends on the concept of IAST in which adsorbed phase is in equilibrium with the gas phase.

We have also used IAST-Sips and IAST-DSL models, which were obtained by substituting pure component Sips and DSL isotherm equations into Eq. (10) followed by its integration. Eqs. (13) and (14) give the reduced spreading pressure for Sips and DSL models, respectively which are also equated for each component and the expressions for Sips and DSL models are given by Eqs. (15) and (16), respectively.

$$P y_i = P_i^0 \left(\pi^*\right) x_i \tag{A.9}$$

where y_i is the mole fraction of component i in gas phase, x_i is the mole fractions of component i adsorbed phase, P is the total pressure of the mixture, P_i^0 (π^*) is the equilibrium gas phase pressure corresponding to solution temperature and spreading pressure, π^*,

$$\pi_i^* = \frac{\pi_i A}{RT} = \int_0^{P_i^0} \frac{q_i^*}{P_i} dP_i \tag{A.10}$$

where π_i^* and π_i are reduced spreading pressure and spreading pressure of component i in the adsorbed phase, respectively, A is the specific surface area of the adsorbent, q_i^* = is the pure component adsorption isotherm equation, and P_i^0 is the standard state pressure of pure component i corresponding to spreading pressure of the mixture.

$$\frac{1}{q_T} = \sum_{i=1}^{N_C} \frac{x_i}{q_i^0\left(P_i^0\right)} \tag{A.11}$$

$$q_i = x_i q_T \tag{A.12}$$

$$\pi_i^* = q_{m,i} c_i \ln\left(1 + b_i \left(P_i^0\right)^{1/c_i}\right) \tag{A.13}$$

$$\pi_i^* = q_{1,m,i} \ln\left(1 + b_{1,i} P_i^0\right) + q_{2,m,i} \ln\left(1 + b_{2,i} P_i^0\right) \tag{A.14}$$

$$q_{m,i} c_1 \ln\left(1 + b_1 \left(\frac{P_1}{x_1}\right)^{1/c_1}\right) = q_{m,2} c_2 \ln\left(1 + b_2 \left(\frac{P_2}{1 - x_1}\right)^{1/c_2}\right) \tag{A.15}$$

IAST based Sips and dual-site Langmuir models

$$\begin{aligned} q_{1,m,1} \ln\left(1 + b_{1,1} \frac{P_1}{x_1}\right) + q_{2,m,1} \ln\left(1 + b_{2,1} \frac{P_1}{x_1}\right) &= q_{1,m,2} \ln\left(1 + b_{1,2} \frac{P_2}{1 - x_1}\right) + \\ &+ q_{2,m,2} \ln\left(1 + b_{2,2} \frac{P_2}{1 - x_1}\right) \end{aligned} \tag{A.16}$$

A MATLAB program is used to calculate xi, by solving the above mentioned equations implicitly.

Selectivity

Selectivity, which is one of the main characteristic properties of adsorbent, can also be determined for CO_2 over N_2 (S_{CO_2}) and is compared with the experimental data obtained from breakthrough curves.

$$S_{CO_2} = \frac{x_{CO_2} / x_{N_2}}{y_{CO_2} / y_{N_2}} \tag{A.17}$$

where x_{CO_2} and S_{N_2} are the mole fractions of CO_2 and N_2 in the adsorbed phase, respectively, and y_{CO_2} and y_{N_2} are the molar ratios of CO_2 and N_2 in the gas phase, respectively.

Thermodynamic study

Three thermodynamic parameters, i.e., integral molar Gibbs free energy, integral molar enthalpy and integral molar entropy were calculated numerically, whose values tell the behavior of the adsorption process (Deng et al., 2012; Ridha and Webley, 2010):

Integral molar Gibbs free energy change for the adsorption process

$$\Delta G = \frac{\Omega}{q} = -\frac{RT \int_0^P q \, d(\ln P)}{q} \tag{A.18}$$

where Ω is the surface potential (kJ mol^{-1}), R is the universal gas constant (kJ mol^{-1} K^{-1}), q is the amount of adsorbate adsorbed (mmol g^{-1}) and T is temperature (K).

Integral molar enthalpy, ΔH (kJ mol^{-1})

$$\Delta H = \frac{\left[\frac{\partial(\Omega/T)}{\partial(1/T)}\right]_P}{q} \tag{A.19}$$

Integral molar entropy change, ΔS (kJ mol^{-1} K^{-1})

$$\Delta S = \frac{-\left(\frac{\partial \Omega}{\partial T}\right)_P}{q} \tag{A.20}$$

Isosteric heat of adsorption for CO_2, Q_{st}, (kJ mol^{-1})

$$Q_{st} = -R\left[\frac{\partial \ln P}{\partial\left(\frac{1}{T}\right)}\right]_{q_e} \tag{A.21}$$